ADVANCED ELECTRONIC MATERIALS
www.advelectronicmat.de

Multishank Thin-Film Neural Probes and Implantation System for High-Resolution Neural Recording Applications

*Sagnik Middya, Alejandro Carnicer-Lombarte, Vincenzo F. Curto, Sam Hilton, Andreas Genewsky, Alexandra L. Rutz, Damiano G Barone, Gabriele S. Kaminski Schierle, Anton Sirota, and George G. Malliaras**

Silicon probes have played a key role in studying the brain. However, the stark mechanical mismatch between these probes and the brain leads to chronic damage in the surrounding neural tissue, limiting their application in research and clinical translation. Mechanically flexible probes made of thin plastic shanks offer an attractive tissue-compatible alternative but are difficult to implant into the brain. They also struggle to achieve the electrode density and layout necessary for the high-resolution applications their silicon counterparts excel at. Here, a multishank high-density flexible neural probe design is presented, which emulates the functionality of stiff silicon arrays for recording from neural population across multiple sites within a given region. The flexible probe is accompanied by a detachable 3D printed implanter, which delivers the probe by means of hydrophobic-coated shuttles. The shuttles can then be retracted with minimal movement and the implanter houses the electronics necessary for in vivo recording applications. Validation of the probes through extracellular recordings from multiple brain regions and histological evidence of minimal foreign body response opens the path to long-term chronic monitoring of neural ensembles.

1. Introduction

Intracortical neural probes have played a pivotal role in developing our understanding of how the brain works. While early probes were designed for use in single brain locations,[1–3] multisite probes have become a more popular alternative. Dense multishank silicon arrays have proven particularly useful in cortical and hippocampal circuits, enabling recording of dozens to hundreds of geometrically localized single neurons and neural ensemble analysis as well as recording cross-laminar local field potentials (LFPs).[4,5] They also enable simultaneous interfacing with different regions of the brain and at different depths. Silicon's compatibility with microfabrication and high Young's modulus has made it a highly suitable material for building shanks that can penetrate the brain and on which metal microelectrodes can be patterned at high spatial resolution.[6] More recently, active electronics based on complementary metal–oxide–semiconductors were integrated with these shanks, offering very high electrode densities.[7–9]

The implantation of any intracortical probe causes insertion trauma which results in the progressive formation of scar tissue that displaces nearby neurons and degrades the probe's performance over time.[10,11] The brain's micromotion from breathing or general body movements also causes shear against the stiff probes and further damages the surrounding tissue. Mechanical mismatch between the soft brain tissue (elastic modulus ≈200 Pa) and stiff probe (170 GPa for silicon) is a key driver of tissue damage after implantation.[12,13] While the use of invasive neural interfaces is gaining traction in research and in clinical practice, finding ways to reduce tissue damage is crucial to ensure this technology reaches widespread use. Modifying silicon probes with softer coatings, lubricated surfaces, or bioactive compounds can partially alleviate the problem.[12,14]

S. Middya, A. Carnicer-Lombarte, V. F. Curto, S. Hilton, A. L. Rutz, D. G. Barone, G. G. Malliaras
Department of Engineering
Electrical Engineering Division
University of Cambridge
Cambridge CB3 0FA, UK
E-mail: gm603@cam.ac.uk

The ORCID identification number(s) for the author(s) of this article can be found under https://doi.org/10.1002/aelm.202200883.

DOI: 10.1002/aelm.202200883

S. Middya, G. S. Kaminski Schierle
Department of Chemical Engineering and Biotechnology
University of Cambridge
Cambridge CB3 0AS, UK

A. Genewsky, A. Sirota
Bernstein Centre for Computational Neuroscience Munich
Faculty of Medicine
Ludwig-Maximilians Universität München
82152 Planegg-Martinsried, Germany

D. G. Barone
Department of Clinical Neurosciences
University of Cambridge
Cambridge CB2 0QQ, UK

However, difficulties in combining these processes with microfabrication techniques limit their applicability. Substitution of silicon with mechanically flexible shanks made of less stiff materials such as polyimide and Parylene C (PaC) is instead becoming a dominant option for the development of stable and biocompatible neural probes.[15–17] Although such compliant probes cannot completely avoid the insertion trauma, they do significantly less damage over the long term.

Flexible probes, however, suffer from one key disadvantage over stiff probes. Implantation into the brain parenchyma becomes challenging due to their tendency to buckle if inserted on their own. To address this challenge, different types of shuttles and implantation strategies have been devised.[14,18] They include 5–10 μm-thick permanent silicon supports integrated with PaC[19] or polyimide[20] flexible probes, sharp hollow needle-like shuttles[21] and removable microwires which are attached with biodegradable adhesives,[14,22,23] or pushing thread like probes inside the brain one by one with a needle.[24,25] Additionally, bioresorbable materials like poly(lactic-*co*-glycolic acid), poly(ethylene glycol) (PEG), chitosan, etc. have been employed to temporarily enhance the stiffness of soft probes.[12] Barring a few exceptions,[26–28] these methods are mostly limited to probes confined to a single location (single shank) and hence, have a narrower scope of application. Recently multishank probes made from PaC were implanted by temporary stiffening the shanks with PEG while leaving the tips exposed.[26,27] These probes combine the virtues of a multisite architecture and small footprint, but the implantation strategy is unsuitable for different probe geometries.

Here, we present an ultrathin (4 μm PaC) flexible intracortical probe with multiple shanks aimed to provide distributed recording of the LFP and multiple single units. The microscale probe was completed with a two-part 3D printed mesoscale implanter comprising of microwire shuttles for delivering the probe in the brain parenchyma and a holder for the probe and electrophysiology amplifier. The construct was designed to allow for easy separation of the shuttles and probe to facilitate removal of the former after implantation. By virtue of its design, the probe not only served to examine neural activity across large brain areas or structures but could also uncover very local cellular features at the same time. The probe also demonstrated promise for stable long-term recordings from deep brain regions. The design features of the probe and implanter contribute to the ecosystem of the new generation of flexible microfabricated recording electrodes for systems neuroscience.

2. Results

2.1. Fabrication and Assembly of the Implantable Device

The flexible probes were made by microfabrication while the implanter was realized by 3D printing. The design of the probe is based on multishank Michigan arrays[29] which are widely used for research.[4,30] A schematic diagram and electrode layout of our probe is shown in Figure S1 in the Supporting Information. The device fabrication was similar to previous examples of neural probes developed in our laboratory.[31,32] An exploded view of the probe is schematically shown in **Figure 1**a. A detailed description of the process is provided in the Experimental Section. Briefly, 2 μm-thick layers of PaC, deposited by chemical vapor deposition (CVD), were used as substrate and insulation. The Au electrodes and interconnects were defined by photolithography and lift-off. The electrodes were coated with poly(3,4-ethylenedioxythiophene) polystyrene sulfonate (PEDOT:PSS) through a sacrificial stencil layer of PaC. Finally, a custom-designed miniature printed circuit board (PCB) with preassembled slim-stack connector was bonded to the flexible probe by anisotropic conducting adhesive. A picture of the completed probe is illustrated in Figure 1a (right, top). Each electrode has an area of 49 μm^2 and their layout in a shank is shown in the bottom right optical image. The probes were characterized by electrochemical impedance spectroscopy (EIS) and a representative spectrum is shown in Figure S2 in the Supporting Information. On an average, the electrodes exhibited an impedance of ≈77 ± 25 kΩ (mean ± standard deviation) at 1 kHz in phosphate buffered saline (PBS).

The multishank design of our probe required multiple shuttles which could deliver each shank simultaneously to the desired location in the brain and later be removed. With that in mind, we designed an implanter that holds multiple 50 μm diameter tungsten microwire shuttles in predefined positions together with the probe during implantation and allow the microwires to be separated and retracted afterward. The microwires were dip-coated with poly(dimethylsiloxane) (PDMS) because the resulting hydrophobic surface reduces insertion trauma.[33] A 3D visualization of the implanter is demonstrated in Figure 1b (left). It consists of a base where the microwires are aligned and fixed in grooves whose pitch matched that of the probe shanks. Breaking off the support at one end (black arrows) exposes the tips of the microwires. The upper arm holds the probe and is attached to the base. Closer views of the parts of the implanter, the base and the probe-holder, are presented in Figure S3a,b in the Supporting Information. Optical image of the assembled and aligned microwires is shown in Figure S3c in the Supporting Information. Figure 1b (right) illustrates an assembled implanter. The flexible probe was fixed to the arm of the implanter and the individual shanks were attached to the microwires with 12% PEG solution. The final probe-implanter assembly is shown in Figure 1c. Since PEG is soluble in water, it dissolves after implantation and releases the probe. The PEG coating was applied just before surgery to avoid excessive drying of the film which results in slow dissolution and release.

During implantation the probe-implanter construct was attached to a stereotaxic frame through a tab on its base. The base containing the microwires was then separated from the probe-holder by breaking off the pillars indicated by blue arrows in Figure 1b (left). The implantation and release of the probe from the microwires were tested in a 0.6% (w/v) agarose phantom with single PaC shanks and microwires. Figure S4a,b in the Supporting Information, respectively show the PaC shank attached to the microwire outside the agarose and after penetrating ≈3 mm. No immediate delamination was observed while lowering the construct. Thereafter, the shank was released by dissolving the PEG with few drops of water and the wires were retracted after around 5 min. The shank was retained in the agarose as observed in Figure S4c in the Supporting Information.

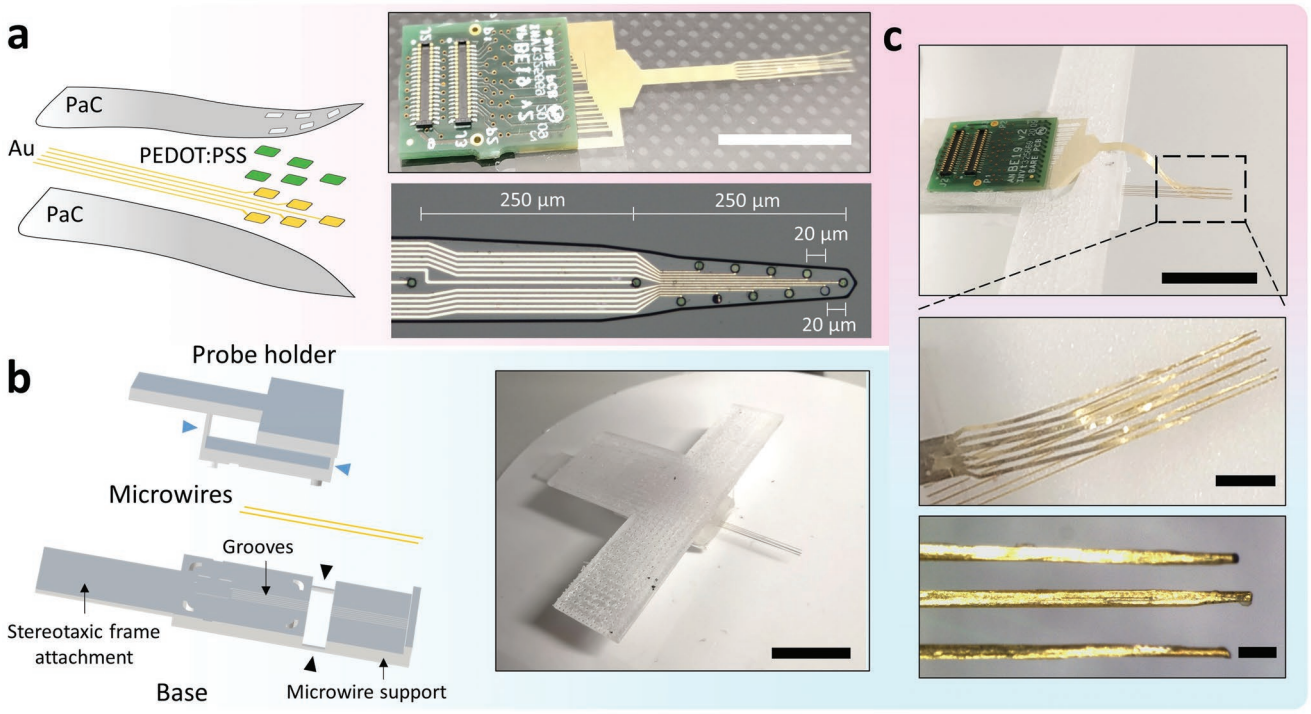

Figure 1. Hybrid fabrication and assembly of the neural probes. a) Left: Exploded schematic view of the neural probe. The PEDOT:PSS-coated Au electrodes are sandwiched between a bottom substrate and top insulation layer, both made of 2 µm-thick PaC. Right: Photograph of the flexible probe bonded to a connector board (top) and optical image of the electrode layout in a shank with the dimensions (bottom). Scale bar—top: 1 cm. b) Left: Schematic diagram of the implanter designed to deliver the flexible probes by temporarily attaching them to 50 µm wire shuttles. The microwires are fixed to grooves within a 3D-printed base and the microwire support is removed (at the black arrowheads) afterward. The probe is mounted on the upper probe holder. The support pillars (blue arrowheads) allow for the separation of the implanter and probe holder portions of the construct after implantation. Right: Photograph of the assembled implanter. Scale bar: 1 cm. c) Top: Photograph of a probe mounted on the implanter and the flexible shanks attached to the microwire shuttles by PEG. Middle and bottom: Magnified optical images of the shanks adhering to the microwires. Scale bars—top: 1 cm; middle: 1 mm; bottom: 200 µm.

The tip of the shank was deliberately positioned slightly behind the tip of the microwire for easy penetration. This is indicated by the arrows in the optical image of a construct in Figure S4d in the Supporting Information and also contributes to the difference in depths (≈60 µm) of the microwire (Figure S4b, Supporting Information) and the shank (Figure S4c, Supporting Information).

2.2. Implantation and Validation of the Multishank Flexible Neural Probes

To validate their functionality, the probes were implanted into the hippocampus of anaesthetized rats as depicted in the cartoon in **Figure 2**a. Fully assembled constructs were mounted on a stereotaxic frame by the tab at their base and slowly lowered so that all shanks reached the hippocampus (depth of 3 mm). Details of the implantation can be found in the Experimental Section. Figure S5a in the Supporting Information shows a closeup view of the implantation site. After implantation, the portion of the microwires and probe remaining outside of the brain was moistened with saline solution to ensure that the PEG dissolved completely. The probe-arm was then secured onto a separate micromanipulator and separated from the base (after cutting at the blue arrows in Figure 1b). The base of the construct containing the microwires was slowly retracted while the probe-arm holding the probe was left on the head of the animal. Figure 2b shows the flexible probes after the microwires were removed. This process achieved ≈80% success rate in implantation, with failure coming from insufficient adhesion between probes and microwires via PEG. The cranial window was sealed with medical silicone and cement. The flexible probe folded down and the probe-arm bundled into a headcap, providing easy and secure access to the miniature connector on the custom head-stage that amplified and digitized signals from the probe (Figure S5b,c, Supporting Information).

Validation of probe functionality was carried out in acute experiments through the triggering of seizure-like activity in the hippocampus. The high-frequency (300–3000 Hz) recording trace from an electrode is shown in Figure 2c. Little notable high-frequency neural activity was observed initially. However, the corresponding time-frequency plot illustrates that some low-frequency activity (alpha, theta, and delta bands, 0–14 Hz) was preserved by the shallow 1% isoflurane anesthesia. Within ≈4 min of delivering of 4-aminopyridine (4-AP), a compound known to induce seizure-like discharges in the brain,[35] neural activity significantly increased across both high and low frequencies. The concentration of isoflurane was subsequently increased to 2.5%, which reversed the seizure-like activity to some extent. Although the high-frequency discharges almost

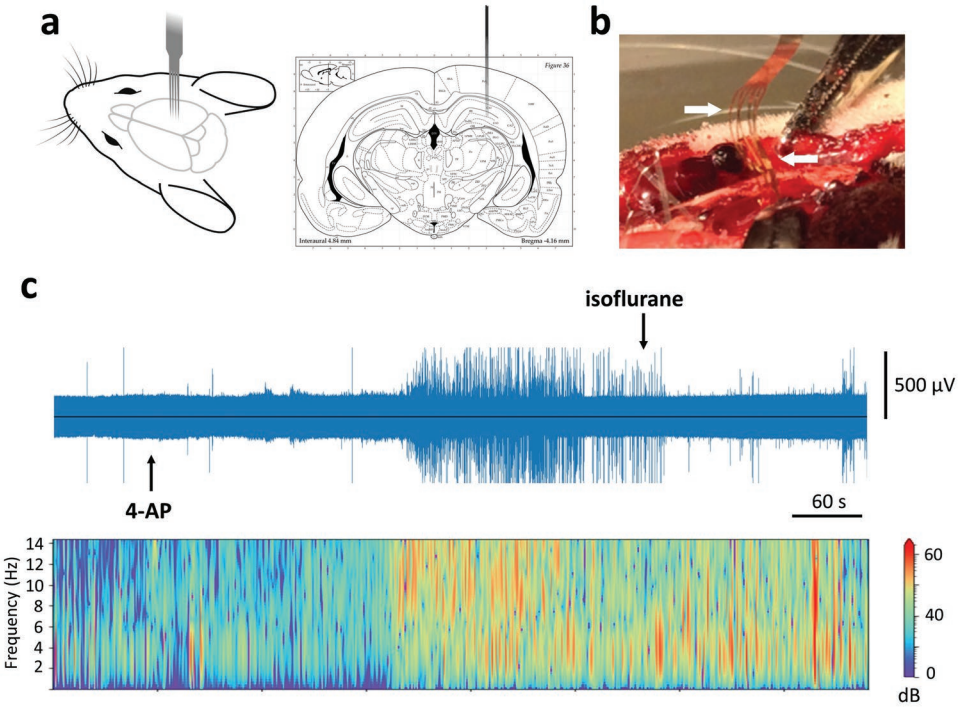

Figure 2. Implantation of multishank flexible probe and neural recording in a hippocampal epilepsy model. a) Cartoon showing the implantation of the probe with the shanks oriented along the AP axis (left) and its location in the brain (right). Annotated image of the coronal section: Reproduced with permission.[34] Copyright 2006, Academic Press. b) Optical image of the implanted probes (pointed by arrows) after the microwires was retracted. c) High-frequency recording trace (top) and time-frequency plot of low-frequency activity (bottom) from an electrode within the hippocampus. The black arrows indicate the injection of the convulsant 4-aminopyridine (4-AP) and increasing the isoflurane anesthetic from 1% to 2.5%, respectively. Injection of 4-AP caused seizure-like activity which could be observed both in the lower and higher frequencies. The ictal activity was then reversed to some degree, by increasing the delivery of isoflurane.

stopped, low-frequency activity remained prominent. These observations are consistent with the expected recording characteristics of penetrating neural probes where the low-frequency signals reported hippocampus-wide activity induced by 4-AP and the high-frequency band read local activation very close to the recording site.

2.3. Combined High Resolution of Neural Recording and Brain Volume Coverage Enabled by the Multishank Flexible Probe Design

We designed the shanks of the probe to be around 300 µm apart, while within each shank, the electrode array covers an area of 200 µm × 100 µm (see Figure S1, Supporting Information). This design was chosen to enable high-resolution recordings of small populations of neurons, while maintaining the ability to interrogate a large volume of brain performing potentially distinct functions or record distributed activity of a large number of single neurons within a single layer, e.g., hippocampal CA1 or cortical layer V. To test our probe's ability to examine single neuron activity across long distances we implanted these into the barrel cortex—a large cortical area containing numerous smaller centers processing sensory activity from individual whiskers. The spontaneous activity was recorded first without carrying out any whisker stimulation. The high-frequency traces from multiple electrodes across different shanks are represented in **Figure 3**a. The corresponding raw recording traces (50 Hz notch filtered) are shown in Figure S6 in the Supporting Information. The signals vary across the array, which is likely explained by the differences in the position of each individual shank with respect to nearby cortical barrels. Different spike amplitudes are also observed in the inter- and intrashank electrodes, with an average of 130 µV (peak to through). The high-frequency signal exhibited a low background noise level of around 12 µV (peak to peak).

Next, we stimulated the whiskers by manually brushing them nonselectively with a cotton swab. During a recording session, we alternated the stimulation between the contralateral and ipsilateral sides every 20 s. The shankwise spike frequencies shown in Figure S7 in the Supporting Information did not reflect any obvious differences during stimulation compared to spontaneous activity. The activity was also nonuniform during certain periods of the 5 min recording session. We performed spike sorting (see Experimental Section) to estimate how many neurons each shank recorded from. The principal component decomposition of spikes recorded from shank 5 (Figure S1, Supporting Information) during contralateral stimulation is shown in Figure 3b. It indicates two distinct neurons, denoted in red and blue, whose spike waveforms from the intrashank electrodes are also shown. The autocorrelograms illustrate the different spiking behaviors of the two identified neurons. However, no statistically significant difference in their firing pattern was observed during whisker stimulation.

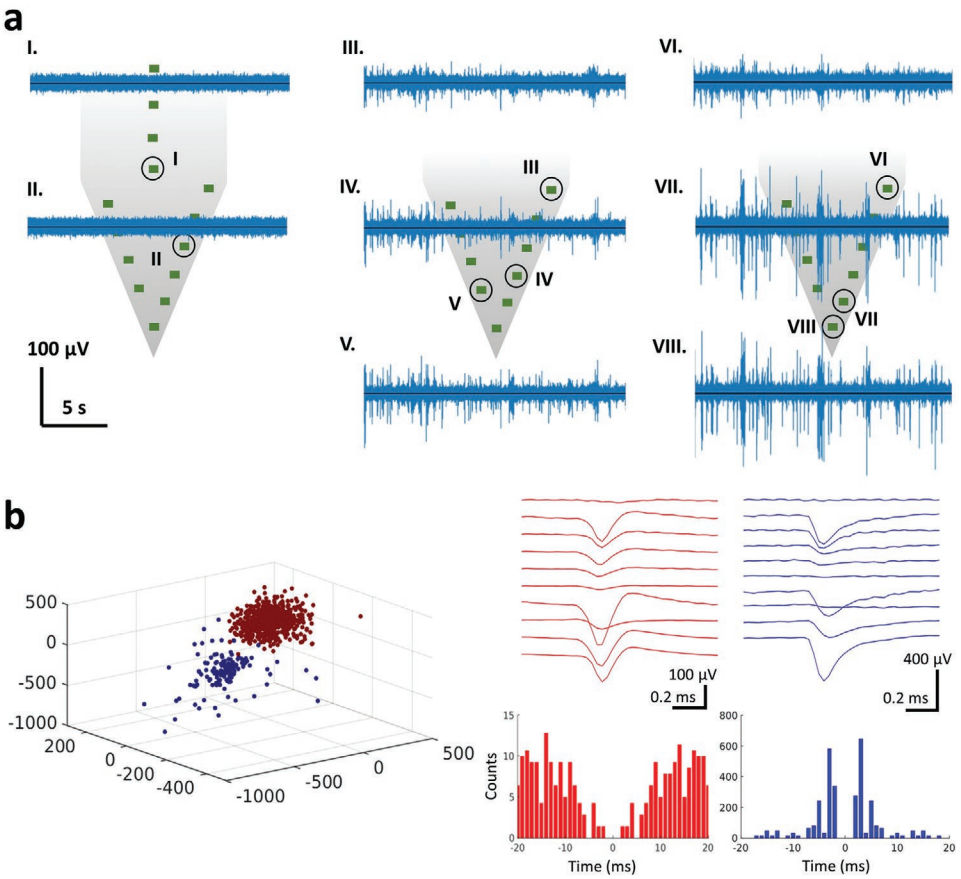

Figure 3. Multishank flexible probes recognize features at the cellular level while simultaneously providing an overview over a wide brain area. a) Snapshot of high-frequency spontaneous activity recorded at different electrodes (numbered I–VIII) on different shanks of a probe implanted in the barrel cortex of a rat. Because of the spatial spread of the electrodes, their recordings varied from one another especially between different shanks. b) Classification of spikes recorded from a shank during whisker contralateral stimulation. Left: 3D representation of the first three principal components of the spikes grouped into red and blue clusters. Right: Spike waveform and corresponding autocorrelogram of each cluster recorded from the intrashank electrodes.

2.4. Minimal Foreign Body Reaction to the Flexible Probes Signify Long-Term Electrophysiology

The probes were implanted in a relatively deep brain region (hippocampus) to test their long-term effects on the surrounding brain tissue. Although the microwire shuttles are removed after implantation, trauma from their insertion would lead to foreign body reaction. We compared the effects of our probes on brain tissue to those of bare 50 µm microwires, implanted in the other hemisphere. **Figure 4**a shows histology images of a horizontal brain section through the hippocampus 28 d after implantation. Although the probes could not be retained through the sectioning process, their footprints are observed in magnified image on the right. The size of the footprint, around 75 µm, corresponds to the tip of the probe. The footprints of the microwires from the opposite hemisphere are shown in Figure 4b. Both our probes and the 50 µm microwires produced relatively little microglial (CD11b/c) and astrocytic glial fibrillary acidic protein (GFAP) activation in the surrounding tissue, which was observed to be mostly limited to a 100 µm radius around the implant (Figure 4a,b). Notably, our thin-film flexible probes produced a significantly lower astrocytic activation than microwires ($p = 0.010$, paired Student's *t*-test), with almost no change compared to healthy naïve brain tissue (Figure S8, Supporting Information). Microglial stain pattern was similar in both our probes and microwires ($p = 0.571$, paired Student's *t*-test, Figure S8, Supporting Information). These results are indicative of a good interface between the electrodes and the surrounding tissue, at least for the duration tested here.

Hippocampal activity was measured over 1 week post implantation from awake animals. Figure 4c shows spontaneous high-frequency activity measured at day 7 from few electrodes across different shanks. The corresponding raw recording traces are shown in Figure S9 in the Supporting Information. Figure 4d illustrates that the mean impedance of the active electrodes increased from ≈300 kΩ at day 1 to around 2 MΩ by day 3 post implantation. These impedance values were maintained over subsequent recording days. A few previously active electrodes became inactive between day 3 and 7, exhibiting impedances greater than 10 MΩ and causing the wide range and standard deviation observed in the plots. Further, spike sorting was performed to identify neurons which were recorded at the electrodes. Figure S10 in the Supporting Information illustrate principal component decomposition and clustering at a shank

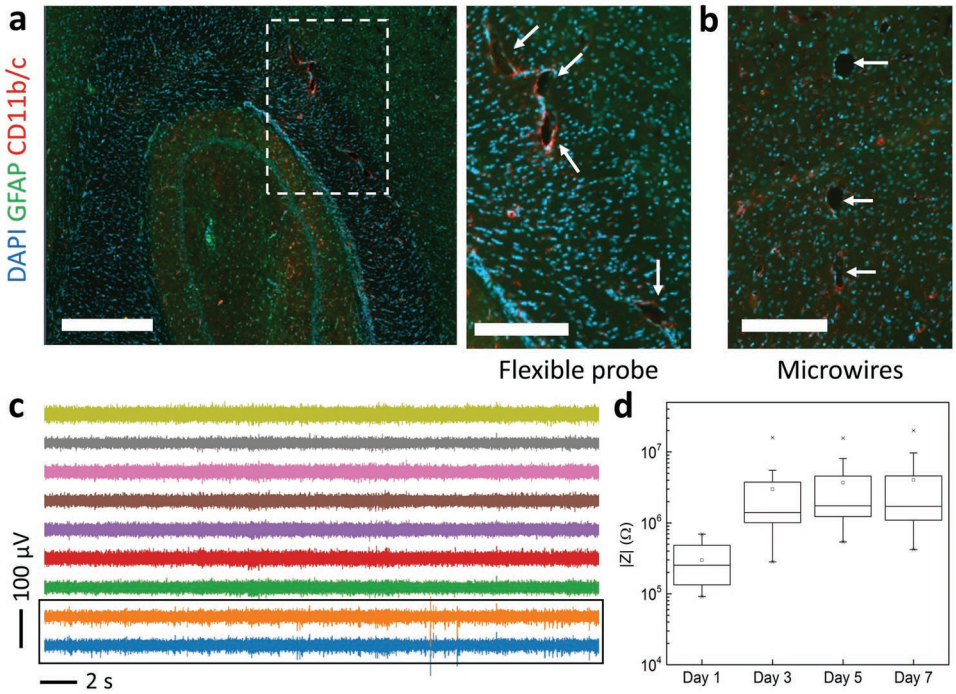

Figure 4. Flexible probes cause minimal tissue damage and enable chronic electrophysiology. a) Left: Histology image of the rat's hippocampus 28 d after implanting the probes, labeled for markers of foreign body reaction: glial scar (GFAP) and CD11b/c positive microglia. The magnified region of interest on the right shows ≈75 µm footprints of multiple shanks (arrows). Scale bars—left: 500 µm; right: 200 µm. b) Histology image from the opposite hemisphere depicting the footprints of the implanted microwires (marked by arrows) for comparison. Scale bar: 200 µm. c) High-frequency spontaneous activity across different electrodes recorded from the hippocampus 1 week after implantation. Spike sorting was performed on the highlighted most active shank (see Figure S10, Supporting Information). d) Variation of the 1 kHz impedances of active electrode during 1 week after implantation.

which comprised of the two channels highlighted in Figure 4c. Four putative neurons characterized by their distinct spike shapes could be identified.

3. Discussion

Prior studies have developed and tested soft intracortical probes and removable shuttles for their implantation.[14,22,23] However, it has been challenging to adopt a multisite architecture with soft probes since they require multiple shuttles for delivery. Recently refs. [26] and [28] demonstrated a shuttle-free method of delivering a multishank flexible probe by temporary stiffening them with PEG coating. As there is no additional shuttle involved, it creates a minimal footprint during implantation. While elegant, this method is likely to encounter limitations in its application for different probe geometries (for example, one with different shank lengths) and depth of possible probe insertion. Moreover, a tightly controlled coating system requires the use of specialized equipment prior to implantation, limiting scalability and translation of this technology into neuroscience laboratories. Here we chose rigid shuttles (tungsten microwires), which are more versatile in that respect and, being coated with hydrophobic PDMS provide minimal tissue damage. Future reduction of the diameter or change of the material of the wire will result in even smaller tissue damage by the shuttles.[28] We use a combination of lithography and 3D printing to translate the multishank silicon probe into a flexible design and create a retractable implanter for its delivery.

Our proposed design can be easily tailored to different applications. The pitch, length, and orientation of the shuttles can be changed with simple modifications to the 3D printed implanter. Its two-part design further aids in the precise alignment of the shuttles (Figure 1b). Similarly, and synergizing with the implanter's customisability, ultrathin probes can be easily designed with different geometries and electrode layouts too. The shuttles are also amenable to different surface coatings used to reduce trauma during implantation. For example, in our case, the microwires were coated with hydrophobic PDMS to lower friction with the surrounding tissue. Other coatings to reduce insertion trauma such as carboxyl terminal self-assembled monolayer (SAM)[22] or lubricant layer[36] can also be applied without significant modification to our implanter. The implanter is also designed such that the microwires can be separated from the probe-arm with minimum movement during surgery and removed easily (Figure 1b). For chronic preparations, the probe-arm can also serve as the base of the headcap which houses the connector PCB.

The hippocampus is a commonly studied target in neuroscience research and a frequent model used to validate the function of new neural probes.[7,37–39] Here, the hippocampal epilepsy model (Figure 2c) exhibits the increase of neural activity induced by 4-AP injection. As the activity spread and reached the electrode's vicinity, stronger high-frequency discharges were recorded. This was associated with enhanced

low-frequency signals, which indicated a significantly higher activity throughout the hippocampus. Increasing the isoflurane concentration reversed the effects of 4-AP, but only partially.

Neuroscience research increasingly focuses on the study of correlations and connectivity between different areas of the brain.[40,41] New advances on the technological side should reflect these needs in order to develop effective tools for research. We tested the capabilities of our probe to record information across large brain regions by implanting our probe into the barrel cortex. In rodents, the barrel cortex is composed of numerous small cortical units (barrels) each processing sensory information from an individual whisker.[42] The unusual structure of the barrel cortex has contributed to making it a popular model in neuroscience research.[43–45]

The electrodes in our case, located between 1 and 1.2 mm below the brain's surface, were placed in the layer 5 of the cortex. This layer receives sensory input from the thalamus[46] and is most active in terms of neural spiking.[47] Based on the dimensions of our multishank probe and the organization of the barrel cortex, we expected each shank to interface with a different barrel column. Deflection of a whisker first activates the respective barrel column and then the response spreads horizontally, depolarizing a large area.[42] Hence, the electrodes are expected to have some degree of correlation among themselves, but more so within each shank which read information from an individual whisker. This was also reflected in our recordings (Figure 3a,b). We expected to see changes in barrel cortex activity in response to whisker stimulation. However, the frequency of spikes was irregular and decreased abruptly during certain stimulation intervals. This precluded any inferences regarding the effect of whisker stimulation.

Addressing the issues faced by conventional rigid probes, especially in chronic electrophysiology, has driven the development of compliant neural probes. With that in mind, our flexible probe was examined in a chronic implantation and electrophysiology setting. Despite the increase in the impedance of the electrodes and some electrodes becoming inactive, the average impedance showed a saturating trend indicating stabilization (Figure 4c,d). Over 4 weeks, the probe showed satisfactory integration with the surrounding tissue, exhibiting minor microglial activation around the implantation site (Figure 4a,b and Figure S8, Supporting Information). Following from ref. [17], although longer implantation (8–12 weeks) would cause stronger glial scarring, the integration of ≈100 µm sized flexible probes as in our case, would not compromise the recording quality significantly. While the chronic electrophysiology experiments carried out in this study were limited to 7 d post-implantation due to back-end connection limitations, the mild long-term inflammatory response generated by the implants suggest that this technology could achieve stable recordings for longer periods of time. Modification of back-end connection designs or the introduction of wireless recording systems could help in achieving this. From a technology validation perspective, recordings over 7 d of implantation were indicative of a robust implantable device architecture and build, and a stable tissue-implant interface enabling neuronal recordings. Similar duration recording experiments are carried out in other studies to test the suitability of new technologies for chronic brain electrophysiology.[32,48–50]

Both the probes and microwires were tethered to the skull while closing the craniotomies. Shear between the rigid microwires and surrounding tissue was expected to cause more damage whereas this effect would be negligible for flexible probes. On the contrary, the microwires showed little effects, probably due to the smaller 50 µm footprint and the comparatively shorter duration of this study.[17]

New design of ultraflexible microfabricated multishank high-density electrodes in combination with minimally invasive delivery system and miniature open-source head-stage opens the path for future systems neuroscience application with multiple advantages over the rigid analogues, including long-term stability of single unit recording in chronic animals and minimal tissue damage.

4. Experimental Section

Microfabrication of Parylene C Multishank Probes: The probes were fabricated by lithography as described by the group previously. First, 2 µm-thick PaC film was deposited on Si wafer by chemical vapor deposition (Speciality Coating Systems, USA). The patterning for the Au layer was performed by photolithography with AZnLOF 2035 photoresist (Microchemicals GmbH, Germany) in a mask aligner (MA/BA 6, Suss MicroTec, Germany). 10 nm Ti and 100 nm Au was deposited by electron beam evaporation (PVD 75, Kurt J Lesker) followed by lift-off in NI 555 (Microchemicals GmbH, Germany). The insulating PaC layer (2 µm) was deposited after that. Outlines of the individual probes were patterned by photolithography with AZ 10xT photoresist and reactive ion etching (RIE) of 4 um PaC (PlasmaPro RIE 80, Oxford Instruments, UK). O_2 (50 sccm), CF_4 (6 sccm), and SF_6 (4 sccm) were used for etching at 60 mTor pressure and 180 W plasma power. Next, 3% Micro-90 detergent solution (Cole-Parmer, UK) was spin coated to form an anti-adhesion layer before depositing the 2 µm-thick sacrificial PaC. The Au electrodes and contacts were exposed by photolithography and etching the top 4 µm PaC, as described before. A SAM of 3-mercaptopropyltrimethoxysilane (MPTMS, Sigma-Aldrich, UK) was formed on the Au by dip-coating in a 10 mM solution (in 75% isopropanol and 25% deionized water) of the same. The SAM of MPTMS improved the adhesion between Au and PEDOT:PSS layer during peeling off the sacrificial PaC layer.[51] A modified PEDOT:PSS solution consisting of PEDOT:PSS (Clevios PH 1000, Heraeus, Germany), 5% (v/v) ethylene glycol, and ≈30 µL of dodecyl benzene sulfonic acid (Sigma-Aldrich, UK) was prepared and sonicated. 1% (v/v) 3-Glycidyloxypropyl)trimethoxysilane (Sigma-Aldrich, UK) was added and filtered through a poly(tetrafluoroethylene) filter (0.45 µm pore size) prior to use. The PEDOT:PSS was spin coated to a ≈250 nm film thickness and baked at 120 °C for 1 min. Finally, the sacrificial PaC was peeled off and the wafer was baked further at 120 °C for 1 h before soaking in deionized (DI) water overnight.

The PaC probes were carefully released from the Si wafer with DI water, transferred onto glass slides and dried on a hotplate. The connector PCB was bonded to the probe's contact pads using an anisotropic conductive adhesive film (ACF) (10 µm particle size, TGP5010, Telephus Inc., Korea). A die bonder (FINEPLACER pico2, Finetech GmbH, Germany) was used for the ACF bonding. The bonded probes were again released from the glass slides with DI water.

Electrochemical Impedance Spectroscopy was carried out with a potentiostat (Autolab Potentiostat, Metrohm AG, Switzerland) using a platinum electrode as the counter electrode. A 10 mV amplitude sinusoidal voltage input with frequencies ranging from 1 Hz to 100 kHz was used for the purpose.

3D Printing and Probe-Implanter Assembly: The implanter has two parts which were made separately. The 3D designs for the parts were prepared in AutoCAD (Autodesk, USA) software. The Asiga MAX X27 (Asiga Europe, Germany) 3D printer and a GR-10 biocompatible resin (Pro3dure) were used. 50 µm-thick Au-coated tungsten microwires

(100211, California Fine Wire Company) were attached with an adhesive to the grooves designed on the base. The upper arm was clipped on top of the base and the microwires were exposed by removing the support (refer to Figure 2b). The microwires were dip coated in uncured PDMS elastomer (10% w/w crosslinker) with a retraction rate of 1 mm s^{-1}. The wires were left overnight at room temperature to allow the elastomer coating to smooth. The wires were then cured in an oven (70 °C, 4 h). The thickness of the coating was determined to be 1–3 µm, by an optical microscope.

The neural probe was mounted on the implanter just before the surgery. The connector PCB at the end of the probe was attached to the probe-arm of the implanter using a double-sided tape. Thereafter, individual shanks were aligned and attached to the microwires by painting 12% PEG solution with a very fine-tip paintbrush. This step was performed under a stereoscope (Nikon SMZ800N, Nikon Metrology Europe, Belgium).

Implantation in Animals: All animal procedures were carried out in accordance with the UK Animals (Scientific Procedures) Act, 1986. Work was approved by the Animal Welfare and Ethical Review Body of the University of Cambridge and by the UK Home Office (project licence number PFF2068BC). A total of 9–250 g Sprague–Dawley rats (Charles River, UK) were used in this study. Surgical procedures were done under anesthesia on a stereotaxic frame, with the animal's body temperature monitored and maintained using a thermal blanket.

For hippocampus experiments, the head of the animal was fixed on a stereotaxic frame and a 3 × 3 mm^2 cranial window was drilled over the hippocampus and the dura was removed. The probe was mounted onto the frame and lowered into the hippocampus CA1 (Bregma coordinates: −3 to −5 mm anterior-posterior (AP), 3 mm medial-lateral (ML), depth of 3 mm). The multiple shanks were aligned along to the sagittal plane. Additionally, a stainless-steel screw was drilled into the cerebrospinal fluid above the cerebellum to act as a recording ground. Once electrophysiology recordings began, 100 mM 4AP in phosphate-buffered saline was then delivered into the hippocampus. Isoflurane anesthesia (2.5% in O_2, lowered to 1.25% prior to and during electrophysiology experiments) was used throughout these experiments. Two animals were used for the initial validation experiments by seizure induction. One animal was used for chronic electrophysiology for 7 d post implantation.

For barrel cortex experiments, the probe was implanted in the barrel cortex region unilaterally (Bregma coordinates −1 to −3 mm AP, 5 mm ML, depth of 1.2 mm). In these experiments, the rat was anaesthetized with 1.5 g kg^{-1} urethane (Sigma-Aldrich, UK) to preserve more neural activity. The whiskers were stimulated manually by rubbing a cotton swab. The stimulations on each side were interleaved and lasted for 20 s. One animal was used for this experiment.

For immunohistochemistry study, five rats were used. Cranial windows were drilled over the hippocampus on both hemispheres. The flexible probe was implanted in one hemisphere as described before and the retracted microwires were implanted on the opposite hemisphere for comparison. The rats were anaesthetized with 2.5% isoflurane (in O_2) during the surgery.

The probes were implanted in the brain at a speed of roughly 300 µm s^{-1} and the microwires were retracted after ≈5 min thus allowing sufficient time for the PEG to dissolve completely.

Electrophysiology and Data Analysis: For neural recordings, the brain screw was used as the reference electrode and was connected to the ground of the recording hardware. The RHD USB interface board and software (Intan Technologies, USA) was used for data acquisition (30 000 Hz sampling rate). The headstage was custom designed around the RHD2164 amplifier chip. The small footprint of the interface PCB, headstage size and low weight of the headstage allows up to two headstages to be used even in a small rodent, like a mouse.

The raw data was exported and processed with self-written Python scripts. For spike information, the raw data was band-pass filtered between 300 and 3000 Hz (2nd order, zero phase Butterworth filter). Spikes were detected from each electrode by setting a threshold of −4.5× standard deviation. The cross-correlation histograms were calculated with 1 ms bins. Spike sorting was performed by principal component analysis based automatic or semiautomatic clustering methods. Recordings from barrel cortex were processed by the standard pipeline of open-source NDmanager plugins, automatic spike sorting by Klustakwik and manual curation using Klusters. K-means clustering was used for the chronic hippocampal recordings.

Immunohistochemistry: The brains were collected 28 d after implantation and transferred to 4% methanol-free paraformaldehyde in PBS-Azide (PBS containing 0.1% sodium azide) and left for 48 h at 4 °C. Then they were transferred to 30% sucrose in PBS-azide and allowed to infuse until tissue sinks (≈72 h). 10 µm sections were cut using cryostat and mounted onto microscope slides. The slides were kept frozen until staining and defrosted for 15 min at room temperature. Tissues were blocked in 5% donkey serum in PBS-Azide for 1 h at room temperature. Subsequently, they were incubated with primary antibodies overnight at 4 °C. The anti-GFAP antibody (ab7260, AbCam, UK) was used at 1/1000 and the anti-CD11b + CD11c antibody [OX42] (ab1211, AbCam, UK) was used at 1/500 in 5% fetal bovine serum (FBS) in PBS-Azide. Tissues were washed three ties with 5% FBS in PBS-Azide. Incubation with secondary antibodies (Donkey anti-Rabbit IgG Alexa Fluor 555 used at 1/500 and Donkey anti-Mouse IgG Alexa Fluor 488 used at 1/2000 dilutions) was carried out next in 5% FBS in PBS-Azide for 3 h at room temperature in the dark. Tissues were washed 5% FBS in PBS-Azide three times and incubated again in Vector TrueVIEW Autofluorescence Quenching Kit for 3 min at room temperature. Finally, they were washed with 5% FBS in PBS-Azide and treated with 1 µg mL^{-1} 4′,6-diamidino-2-phenylindole (DAPI) (in 5% FBS in PBS-Azide) for 5 min. ProLong Gold Antifade Mountant (Thermofisher, UK) coverslips were used to cover the tissue. The imaging was performed in a Zeiss Axioscan 7 microscope.

Stain intensity quantification was carried out in the ZEN Lite software (Zeiss). Stain intensity for GFAP and CD11b/c was measured in a 100 µm diameter circular area around implants, in horizontal brain sections at hippocampal depth. For each animal, stain intensity values were calculated as the average of three flexible probes and three microwires. Three measurements were also taken for each animal in naive hippocampal tissue lacking implants, which were used to calculate the fold change of stain intensity in flexible probes and microwires compared to naïve brain stain. Quantification was carried out on $n = 4$ rats and statistical comparison was done via paired Student's t-test.

Supporting Information

Supporting Information is available from the Wiley Online Library or from the author.

Acknowledgements

S.M., A.C.-L., and V.F.C. contributed equally to this work. This work was funded by the European Union's Horizon 2020 research and innovation programme under grant agreement no. 732032 (BrainCom). S.M. acknowledges funding from the Cambridge Trust, University of Cambridge. A.L.R. acknowledges support from the Whitaker International Fellows and Scholars Program and the European Commission's Horizon 2020 Marie Sklodowska–Curie Individual Fellowship BRAIN CAMO (No. 797506). A.C.-L. acknowledges support from the Wellcome Trust and University of Cambridge Junior Interdisciplinary Fellowship and from the University of Cambridge Borysiewicz Interdisciplinary Fellowship. G.S.K.S. acknowledges funding from the Wellcome Trust (065807/Z/01/Z) (203249/Z/16/Z), the UK Medical Research Council (MRC) (MR/K02292X/1), Alzheimer Research UK (ARUK) (ARUK-PG013-14), Michael J. Fox Foundation (16238 and 022159) and Infinitus China Ltd.

Conflict of Interest

The authors declare no conflict of interest.

Data Availability Statement

The data that support the findings of this study are available from the corresponding author upon reasonable request.

Keywords

flexible probes, implanters, microwire shuttles, multishanks, neural recording

Received: August 5, 2022
Revised: November 14, 2022
Published online: December 23, 2022

[1] D. H. Hubel, *Science* **1957**, *125*, 549.
[2] B. L. McNaughton, J. O'Keefe, C. A. Barnes, *J. Neurosci. Methods* **1983**, *8*, 391.
[3] K. D. Wise, J. B. Angell, A. Starr, *IEEE Trans. Biomed. Eng.* **1970**, *17*, 238.
[4] G. Buzsáki, *Nat. Neurosci.* **2004**, *7*, 446.
[5] J. Csicsvari, B. Jamieson, K. D. Wise, G. Buzsáki, *Neuron* **2003**, *37*, 311.
[6] E. M. Maynard, C. T. Nordhausen, R. A. Normann, *Electroencephalogr. Clin. Neurophysiol.* **1997**, *102*, 228.
[7] J. J. Jun, N. A. Steinmetz, J. H. Siegle, D. J. Denman, M. Bauza, B. Barbarits, A. K. Lee, C. A. Anastassiou, A. Andrei, Ç. Aydın, M. Barbic, T. J. Blanche, V. Bonin, J. Couto, B. Dutta, S. L. Gratiy, D. A. Gutnisky, M. Häusser, B. Karsh, P. Ledochowitsch, C. M. Lopez, C. Mitelut, S. Musa, M. Okun, M. Pachitariu, J. Putzeys, P. D. Rich, C. Rossant, W. Sun, K. Svoboda, et al., *Nature* **2017**, *551*, 232.
[8] B. C. Raducanu, R. F. Yazicioglu, C. M. Lopez, M. Ballini, J. Putzeys, S. Wang, A. Andrei, V. Rochus, M. Welkenhuysen, N. van Helleputte, S. Musa, R. Puers, F. Kloosterman, C. van Hoof, R. Fiáth, I. Ulbert, S. Mitra, *Sensors* **2017**, *17*, 2388.
[9] N. A. Steinmetz, C. Aydin, A. Lebedeva, M. Okun, M. Pachitariu, M. Bauza, M. Beau, J. Bhagat, C. Böhm, M. Broux, S. Chen, J. Colonell, R. J. Gardner, B. Karsh, F. Kloosterman, D. Kostadinov, C. Mora-Lopez, J. O'Callaghan, J. Park, J. Putzeys, B. Sauerbrei, R. J. J. van Daal, A. Z. Vollan, S. Wang, M. Welkenhuysen, Z. Ye, J. T. Dudman, B. Dutta, A. W. Hantman, K. D. Harris, et al., *Science* **2021**, *372*, eabf4588.
[10] R. Chen, A. Canales, P. Anikeeva, *Nat. Rev. Mater.* **2017**, *2*, 16093.
[11] F. Lotti, F. Ranieri, G. Vadalà, L. Zollo, G. Di Pino, *Front. Neurosci.* **2017**, *11*, 497.
[12] A. Lecomte, E. Descamps, C. Bergaud, *J. Neural Eng.* **2018**, *15*, 031001.
[13] K. M. Szostak, L. Grand, T. G. Constandinou, *Front. Neurosci.* **2017**, *11*, 665.
[14] N. Sharafkhani, A. Z. Kouzani, S. D. Adams, J. M. Long, G. Lissorgues, L. Rousseau, J. O. Orwa, *J. Neurosci. Methods* **2022**, *365*, 109388.
[15] S. P. Lacour, G. Courtine, J. Guck, *Nat. Rev. Mater.* **2016**, *1*, 16063.
[16] J. Rivnay, H. Wang, L. Fenno, K. Deisseroth, G. G. Malliaras, *Sci. Adv.* **2017**, *3*, e1601649.
[17] M. Vomero, F. Ciarpella, E. Zucchini, M. Kirsch, L. Fadiga, T. Stieglitz, M. Asplund, *Biomaterials* **2022**, *281*, 121372.
[18] N. V. Apollo, B. Murphy, K. Prezelski, N. Driscoll, A. G. Richardson, T. H. Lucas, F. Vitale, *J. Neural Eng.* **2020**, *17*, 041002.
[19] D. Egert, R. L. Peterson, K. Najafi, in *2011 16th Int. Solid-State Sensors, Actuators and Microsystems Conf.*, IEEE, Piscataway, NJ, USA **2011**, pp. 198–201.
[20] K.-K. Lee, J. He, A. Singh, S. Massia, G. Ehteshami, B. Kim, G. Raupp, *J. Micromech. Microeng.* **2003**, *14*, 32.
[21] B. J. Kim, J. T. W. Kuo, S. A. Hara, C. D. Lee, L. Yu, C. A. Gutierrez, T. Q. Hoang, V. Pikov, E. Meng, *J. Neural Eng.* **2013**, *10*, 045002.
[22] T. D. Y. Kozai, D. R. Kipke, *J. Neurosci. Methods* **2009**, *184*, 199.
[23] A. Richter, Y. Xie, A. Schumacher, S. Löffler, R. D. Kirch, J. Al-Hasani, D. H. Rapoport, C. Kruse, A. Moser, V. Tronnier, S. Danner, U. G. Hofmann, *Front. Neuroeng.* **2013**, *6*, 6.
[24] L. Luan, X. Wei, Z. Zhao, J. J. Siegel, O. Potnis, C. A. Tuppen, S. Lin, S. Kazmi, R. A. Fowler, S. Holloway, A. K. Dunn, R. A. Chitwood, C. Xie, *Sci. Adv.* **2017**, *3*, e1601966.
[25] E. Musk, Neuralink, *J. Med. Internet Res.* **2019**, *21*, e16194.
[26] K. Srikantharajah, R. Medinaceli Quintela, K. Doerenkamp, B. M. Kampa, S. Musall, M. Rothermel, A. Offenhäusser, *Sci. Rep.* **2021**, *11*, 18920.
[27] X. Wang, A. W. Hirschberg, H. Xu, Z. Slingsby-Smith, A. Lecomte, K. Scholten, D. Song, E. Meng, *J. Microelectromech. Syst.* **2020**, *29*, 499.
[28] Z. Zhao, X. Li, F. He, X. Wei, S. Lin, C. Xie, *J. Neural Eng.* **2019**, *16*, 035001.
[29] K. D. Wise, *IEEE Eng. Med. Biol. Mag.* **2005**, *24*, 22.
[30] D. R. Kipke, W. Shain, G. Buzsáki, E. Fetz, J. M. Henderson, J. F. Hetke, G. Schalk, *J. Neurosci.* **2008**, *28*, 11830.
[31] D. Khodagholy, T. Doublet, M. Gurfinkel, P. Quilichini, E. Ismailova, P. Leleux, T. Herve, S. Sanaur, C. Bernard, G. G. Malliaras, *Adv. Mater.* **2011**, *23*, H268.
[32] D. Khodagholy, J. N. Gelinas, T. Thesen, W. Doyle, O. Devinsky, G. G. Malliaras, G. Buzsáki, *Nat. Neurosci.* **2015**, *18*, 310.
[33] W. Jensen, K. Yoshida, U. G. Hofmann, *IEEE Trans. Biomed. Eng.* **2006**, *53*, 934.
[34] G. Paxinos, C. Watson, *The Rat Brain in Stereotaxic Coordinates*, 6th ed., Academic Press, London, UK **2006**.
[35] M. Szente, A. Baranyi, *Brain Res.* **1987**, *413*, 368.
[36] Y. Lee, H. Shin, D. Lee, S. Choi, I.-J. Cho, J. Seo, *Adv. Sci.* **2021**, *8*, 2100231.
[37] A. Bragin, J. Hetke, C. L. Wilson, D. J. Anderson, J. Engel, G. Buzsáki, *J. Neurosci. Methods* **2000**, *98*, 77.
[38] C. M. Proctor, A. Slézia, A. Kaszas, A. Ghestem, I. del Agua, A.-M. Pappa, C. Bernard, A. Williamson, G. G. Malliaras, *Sci. Adv.* **2018**, *4*, eaau1291.
[39] H. Shin, Y. Son, U. Chae, J. Kim, N. Choi, H. J. Lee, J. Woo, Y. Cho, S. H. Yang, C. J. Lee, I.-J. Cho, *Nat. Commun.* **2019**, *10*, 3777.
[40] A. P. Alivisatos, M. Chun, G. M. Church, R. J. Greenspan, M. L. Roukes, R. Yuste, *Neuron* **2012**, *74*, 970.
[41] C. Lewis, C. Bosman, P. Fries, *Curr. Opin. Neurobiol.* **2015**, *32*, 68.
[42] C. C. H. Petersen, *Neuron* **2007**, *56*, 339.
[43] P. J. Rousche, D. S. Pellinen, D. P. Pivin, J. C. Williams, R. J. Vetter, D. R. Kipke, *IEEE Trans. Biomed. Eng.* **2001**, *48*, 361.
[44] K. Lee, J. He, R. Clement, S. Massia, B. Kim, *Biosens. Bioelectron.* **2004**, *20*, 404.
[45] J. Lee, I. Ozden, Y.-K. Song, A. V. Nurmikko, *Nat. Methods* **2015**, *12*, 1157.
[46] C. C. H. Petersen, *Nat. Rev. Neurosci.* **2019**, *20*, 533.
[47] R. T. Narayanan, D. Udvary, M. Oberlaender, *Front. Neuroanat.* **2017**, *11*, 91.
[48] A. L. Juavinett, G. Bekheet, A. K. Churchland, *eLife* **2019**, *8*, e47188.
[49] G. Hong, T.-M. Fu, M. Qiao, R. D. Viveros, X. Yang, T. Zhou, J. M. Lee, H.-G. Park, J. R. Sanes, C. M. Lieber, *Science* **2018**, *360*, 1447.
[50] R. Garcia-Cortadella, G. Schwesig, C. Jeschke, X. Illa, A. L. Gray, S. Savage, E. Stamatidou, I. Schiessl, E. Masvidal-Codina, K. Kostarelos, A. Guimerà-Brunet, A. Sirota, J. A. Garrido, *Nat. Commun.* **2021**, *12*, 211.
[51] V. F. Curto, M. P. Ferro, F. Mariani, E. Scavetta, R. M. Owens, *Lab Chip* **2018**, *18*, 933.